Structure of an Oligodeoxynucleotide Containing a Butadiene Oxide-Derived N1 Beta-Hydroxyalkyl Deoxyinosine Adduct in the Human *N-ras* Codon 61 Sequence†

Tandace A. Scholdberg,[#] W. Keither Merritt,[#] Stephen M. Dean,[#] Agnieska Kowalcyzk,[#] Constance M. Harris,[#] Thomas M. Harris,[#] Carmelo J. Rizzo,[#] R. Stephen Lloyd,[‡] and Michael P. Stone*[,#]

Department of Chemistry, Center in Molecular Toxicology, Vanderbilt-Ingram Cancer Center, Vanderbilt University, Nashville, Tennessee 37235, and Center for Research on Environmental and Occupational Toxicology, Oregon Health and Science University, 3181 SW Sam Jackson Park Road, L606, Portland, Oregon 97239-3098

Received August 13, 2004; Revised Manuscript Received October 26, 2004

ABSTRACT: The solution structure of the N1-(1-hydroxy-3-buten-2(*S*)-yl)-2′-deoxyinosine adduct arising from the alkylation of adenine N1 by butadiene epoxide (BDO), followed by deamination to deoxyinosine, was determined, in the oligodeoxynucleotide d(CGGACXAGAAG)·d(CTTCTCGTCCG). This oligodeoxynucleotide contained the BDO adduct at the second position of codon 61 of the human *N-ras* protooncogene, and was named the *ras61 S*-N1−BDO-(61,2) adduct. ^{1}H NMR revealed a weak C^5 H1′ to X^6 H8 NOE, followed by an intense X^6 H8 to X^6 H1′ NOE. Simultaneously, the X^6 H8 to X^6 H3′ NOE was weak. The resonance arising from the T^{17} imino proton was not observed. ^{1}H NOEs between the butadiene moiety and the DNA positioned the adduct in the major groove. Structural refinement based upon a total of 364 NOE-derived distance restraints yielded a structure in which the modified deoxyinosine was in the high syn conformation about the glycosyl bond, and T^{17}, the complementary nucleotide, was stacked into the helix, but not hydrogen bonded with the adducted inosine. The refined structure provided a plausible hypothesis as to why this N1 deoxyinosine adduct strongly coded for the incorporation of dCTP during trans lesion DNA replication, both in *Escherichia coli* [Rodriguez, D. A., Kowalczyk, A., Ward, J. B. J., Harris, C. M., Harris, T. M., and Lloyd, R. S. (2001) *Environ. Mol. Mutagen. 38,* 292−296], and in mammalian cells [Kanuri, M., Nechev, L. N., Tamura, P. J., Harris, C. M., Harris, T. M., and Lloyd, R. S. (2002) *Chem. Res. Toxicol. 15,* 1572−1580]. Rotation of the N1 deoxyinosine adduct into the high syn conformation may facilitate incorporation of dCTP via Hoogsteen-type templating with deoxyinosine, thus generating A-to-G mutations.

1,3-Butadiene (CAS RN 106-99-0) (BD)[1] is used in the manufacture of styrene-butadiene rubber (SBR) (*1*, *2*); several billion pounds per year are produced in the United States. It is a combustion product from automobile emissions (*3*) and cigarette smoke (*4*). BD is genotoxic and is a carcinogen in rodents, particularly in mice (*5*−*7*) and also in rats (*8*). Recently, BD was classified by the United States Environmental Protection Agency as "carcinogenic to humans by inhalation" (*9*). The International Agency for Cancer Research (IARC) lists BD as a "probable human carcinogen" (Group 2A) (*10*). Chronic human exposure in the SBR industry may induce genotoxic effects (*11*−*13*) and is correlated with increased risk for leukemia (*1*, *14*−*22*).

BD is epoxidized primarily by cytochrome P450 2E1, but also by cytochrome P450 2A6, to form 1,2-epoxy-3-butenes (BDO) (Scheme 1) (*23*, *24*). BDO is a reactive electrophile that can potentially alkylate nucleophilic sites in DNA, including the imine nitrogen at N1 of deoxyadenosine. Alkylation could occur from either carbon atom of the oxirane; attack by the interior carbon atom, designated C_β, yields two possible stereoisomers of the N1-(1-hydroxy-3-buten-2-yl)-2′-deoxyadenosine adduct. These initially formed N1-dA adducts are prone to deamination (*25*), which yields two possible stereoisomeric N1-(1-hydroxy-3-buten-2-yl)-2′-deoxyinosine adducts (Scheme 2).

Deamination of dA represents a promutagenic event because during DNA replication, the resulting dI nucleotide is recognized as dG and preferentially pairs with incoming dCTP during DNA replication. However, in the N1-(1-hydroxy-3-buten-2-yl)-2′-deoxyinosine adducts, dI is alkylated at the N1 position, thus blocking base pairing with dCTP. Nevertheless, when ligated into the single-stranded vector M13mp7L2 that was used to transfect repair-deficient AB2480 (*uvrA*-, *recA*-) and SOS-proficient AB1157 *Escherichia coli*, the N1-(1-hydroxy-3-buten-2(*S*)-yl)-2′-deoxyinosine adduct strongly coded for incorporation of dCTP (*26*).

† This work was supported by NIH Grant ES-05509 (M.P.S.). Funding for the NMR spectrometers was supplied by Vanderbilt University, by NIH Grant RR-05805, and the Vanderbilt Center in Molecular Toxicology, ES-00267. The Vanderbilt-Ingram Cancer Center is supported by NIH Grant CA-68485.

* To whom correspondence should be addressed. Telephone: 615-322-2589; fax: 615-322-7591; e-mail: michael.p.stone@vanderbilt.edu.

[#] Vanderbilt University.

[‡] Oregon Health and Science University.

[1] Abbreviations: BD, butadiene; BDE, 3,4-epoxy-1,2-butanediol; BDO, butadiene monoepoxide (1,2-epoxy-3-butene); BDO_2, butadiene diepoxide (1,2:3,4-diepoxybutane); CPK, Corey-Pauling-Koltun space-filling models; DQF-COSY, double-quantum filtered correlation spectroscopy; HMBC, heteronuclear multiple bond correlation spectroscopy; R_1^x, sixth root residual; rMD, restrained molecular dynamics; rmsd, root-mean-square deviation; SBR, styrene-butadiene rubber; TOCSY, total correlation spectroscopy; TPPI, time-proportional phase increment.

10.1021/bi0482452 CCC: $30.25
Published on Web 02/09/2005

Scheme 1: (A) Cytochrome P450-Mediated Epoxidation of Butadiene to Mono- and Di-Epoxides. (B) Alkylation of Deoxyadenosine N1 by C_β of Butadiene Mono-Epoxide (BDO) and Subsequent Deamination Yields the N1-(1-Hydroxy-3-buten-2-yl)-2′-Deoxyinosine Adduct

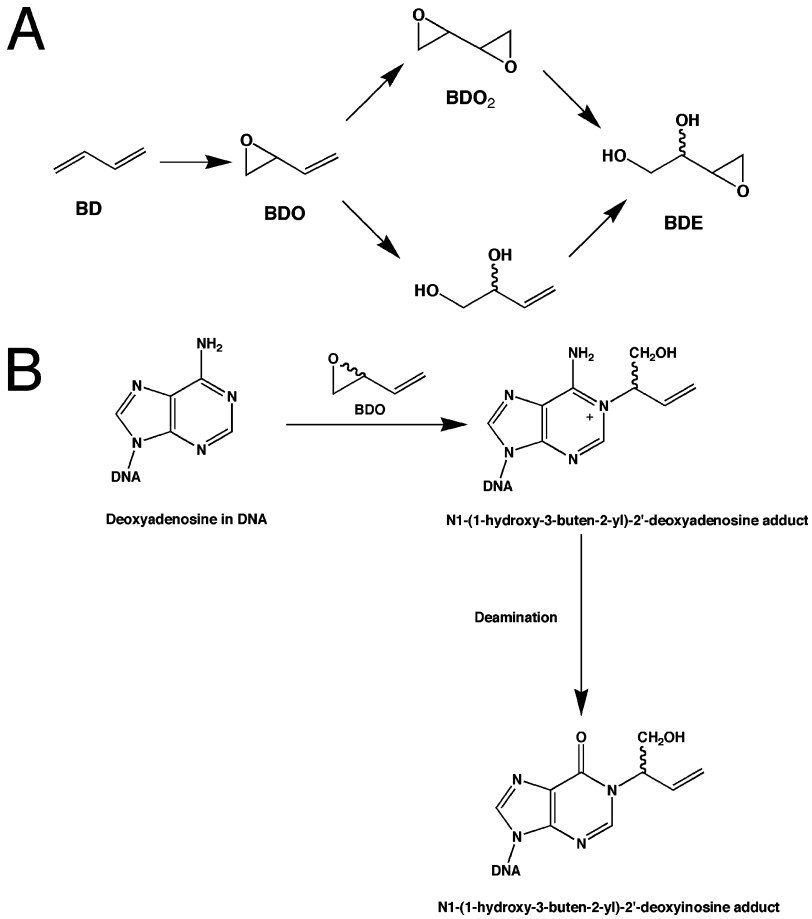

Scheme 2: The Adducted *ras61* Oligodeoxynucleotide, the Chemical Structure of the N1-(1-Hydroxy-3-buten-2(*S*)-yl)-2′-Deoxyinosine Adduct, and Nomenclature[2]

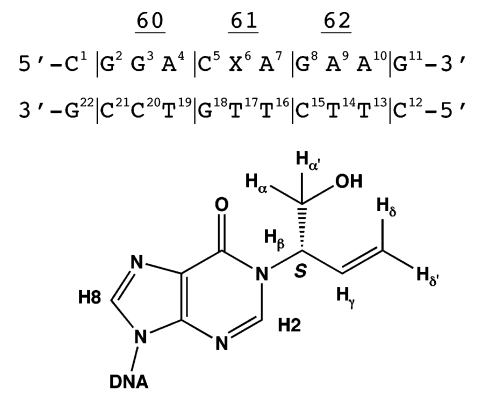

Studies of this adduct in COS-7 cells yielded similar results (*27*). A structural hypothesis was proposed, which posited that incorporation of dCTP opposite the N1-(1-hydroxy-3-buten-2(*S*)-yl)-2′-deoxyinosine adduct occurred as a result of rotation of the N1-adducted dI into the syn conformation about the glycosyl bond, thus enabling formation of a protonated dI·dC Hoogsteen pair during translesion synthesis (*27*).

Accordingly, the N1-(1-hydroxy-3-buten-2(*S*)-yl)-2′-deoxyinosine adduct was site-specifically incorporated into the *ras61* oligodeoxynucleotide (*28*). The resulting oligodeoxynucleotide, 5′-d(CGGACXAGAAG)-3′·5′-d(CTTCTTGTC-CG)-3′, contained the N1-(1-hydroxy-3-buten-2(*S*)-yl)-2′-deoxyinosine adduct at the second position of codon 61. This was named the *ras61 S*-N1−BDO-(61,2) adduct (Scheme 2). The solution structure, as refined from NMR data, confirmed the rotation of the glycosyl bond of the *S*-N1−BDO-(61,2) adduct into the high syn conformation, thus placing the butadiene moiety into the major groove. The complementary dT remained intrahelical at the adduct site. The results support the hypothesis that the tendency of the *ras61 S*-N1−BDO-(61,2) adduct to code for incorporation of dCTP may be attributed to the propensity of this adduct to form a protonated Hoogsteen pairing interaction with dCTP during trans lesion replication. The deamination of initially formed N1 alkylation products arising from BDO, and possibly other electrophiles arising from metabolism of butadiene, may represent the source of *H-ras* specific A-to-G mutations observed in vivo (*27*).

MATERIALS AND METHODS

Oligodeoxynucleotide Synthesis. The unmodified oligodeoxynucleotides 5′-d(CGGACAAGAAG)-3′ and 5′-d(CT-

[2] The definitions of the prochiral protons at C_α of the BDO adduct are based upon the Cahn, Ingold, and Prelog nomenclature. The proton H_α is defined as the pro-*R* proton at C_α; $H_{\alpha'}$ is defined as the pro-*S* proton at C_α. At C_δ, H_δ was defined as the proton in the trans configuration with respect to H_γ, whereas $H_{\delta'}$ was defined as the proton in the cis configuration.

TCTTGTCCG)-3′ were synthesized by the Midland Certified Reagent Co. (Midland, TX) and purified by anion-exchange chromatography. The concentrations of these single-stranded unmodified oligonucleotides were determined from calculated extinction coefficients at 260 nm; the concentration of the modified single-stranded oligodeoxynucleotide was determined from the calculated extinction coefficient of 9.08 $\times$ 10^4 cm^{-1} at 260 nm (*29*). To prepare the modified duplex 5′-d(CGGACXAGAAG)-3′•5′-d(CTTCTTGTCCG)-3′ an excess of unmodified strand was annealed with the *S*-N1−BDO-(61,2) modified strand (*30*), in a buffer consisting of 10 mM NaH_2PO_4, 0.1 M NaCl, and 50 μM Na_2EDTA at pH 7.0. The solution was heated at 95 °C for 5 min and then allowed to cool slowly to room temperature. The resulting mixture of single-stranded and duplex DNA was equilibrated in 10 mM NaH_2PO_4, 0.1 M NaCl, 50 μM Na_2EDTA at pH 7.0 on a column containing DNA Grade Biogel hydroxylapatite (Bio-Rad Laboratories, Hercules, CA). The DNA was eluted off the hydroxylapatite with a gradient from 10 to 200 mM NaH_2PO_4, pH 7.0, to separate excess single-stranded from duplex DNA. The duplex was lyophilized, resuspended in 1 mL of H_2O, and desalted on a Sephadex G-25 column. The sample was lyophilized.

NMR Spectroscopy. The *S*-N1−BD sample was prepared at a DNA strand concentration of 1.3 mM dissolved in 300 μL of 10 mM NaH_2PO_4, 10 mM NaCl, 50 μM EDTA buffer at pH 7.0. For observation of nonexchangeable protons, it was dissolved in 99.96% D_2O. The temperature was controlled at 22 °C ± 0.5 °C. For observation of exchangeable protons, the sample was dissolved in 9:1 H_2O/D_2O. The temperature was controlled at 10 ± 0.5 °C.

To derive distance restraints, NOESY experiments were acquired at mixing times of 200, 250, 300, and 350 ms at a ^1H frequency of 800.23 MHz. For examination of exchangeable protons, experiments were carried out using a field gradient Watergate pulse sequence for water suppression (*31*). The spectra were recorded at 20 °C and 150 ms mixing time. These experiments were recorded with 1024 real data points in the d1 dimension and 2048 real data points in the d2 dimension. A relaxation delay of 2.0 s was used. TOCSY experiments were performed with mixing times of 90 and 150 ms, utilizing the MLEV17 sequence (*32*). The data in the d1 dimension were zero-filled to give a matrix of 1024 $\times$ 2048 real points. A sine-bell squared apodization with a 90° phase shift and a skew factor of 1.0 was used in both dimensions. Data were processed using FELIX (Accelrys, Inc., San Diego, CA) on Octane workstations (Silicon Graphics, Inc., Mountain View, CA).

Structural Refinement. Classical A-DNA and B-DNA were used as reference structures to create starting structures (*33*). The butadiene adduct was constructed using the BUILDER module of INSIGHT II (Accelrys, Inc.). The reference structures were energy-minimized by the conjugate gradients algorithm for 200 iterations without experimental restraints to give starting structures IniA and IniB used for subsequent relaxation matrix analysis and MD calculations. The program X-PLOR (*34*) was used for potential energy minimization. The CHARMM force field was utilized.

NOESY cross-peak intensities were determined by volume integration. These were combined with intensities generated from complete relaxation matrix analysis of a starting DNA structure to generate a hybrid intensity matrix (*35*, *36*) which was optimized using MARDIGRAS (*37*−*39*). Calculations run at correlation times of 2, 3, and 4 ns for both the sugar and base protons yielded 18 sets of distances. Average distances and standard deviations calculated from these data were used as bounds for distance restraints. These were divided into classes on the basis of confidence.

Restrained Molecular Dynamics Calculations. The calculations were in vacuo. The electrostatic term used a reduced charge set of partial charges and a distance-dependent dielectric constant of 4.0. The van der Waals term was approximated using the Lennard-Jones potential energy function. The effective energy function included distance and dihedral restraints, which were in the form of square-well potentials (*40*). Bond lengths involving hydrogen were fixed with the SHAKE algorithm (*41*).

Random velocities fitting a Maxwell−Boltzmann distribution at 2500 K were assigned. Temperature was controlled by coupling to a bath with a coupling constant of 0.05 ps (*42*). Ten randomly seeded structures were calculated from each starting structure. Calculations were carried out for 3000 steps at 2500 K, then cooled to 300 K over 5000 steps, and continued at 300 K for an additional 15 000 steps. An initial force constant of 50.0 kcal mol^{-1} was used for class 1 distance restraints. Throughout the calculations, the force constants for classes 2, 3, 4, and 5 were set to 90, 80, 70, and 60%, respectively, of the value for class 1. The initial value of the force constant for the base pairing restraints was set at 50.0 kcal mol^{-1}. The force constants were maintained at the initial value for the first 10 000 steps; class 1 force constants were increased to 200 kcal mol^{-1}, and base pairing force constants were increased to 150 kcal mol^{-1} over the next 10 000 steps. The force constants were maintained for 17 000 steps, scaled down to 70 and 50 kcal mol^{-1} for class 1 and base pairing restraints, respectively, over 3000 steps and remained at these values for the final 10 000 steps. Structure coordinates were archived every 0.1 ps over the final 10 ps. Structure coordinates extracted from the final 4 ps were averaged and energy-minimized for 200 iterations using the conjugate gradients algorithm.

Back-calculation of ^1H NOE data was performed using CORMA (v. 4.0) (*43*). Helicodial parameters were examined using 3DNA (*44*).

RESULTS

Nonexchangeable Protons. An expansion of the NOESY spectrum showing cross-peaks between base aromatic and deoxyribose anomeric protons is shown in Figure 1. A significant observation was the weak C^5 H1′ to X^6 H8 sequential NOE, followed by an intense X^6 H8 to X^6 H1′ NOE. Simultaneously, the X^6 H8 to X^6 H3′ NOE was unusually weak. This pattern was clearly observed when integrated volumes for these NOESY cross-peaks were plotted as a function of nucleotide position (Figure 2). In the complementary strand, a complete set of sequential NOE connectivities was observed. In contrast to the adducted strand, the intensities of all of the sequential NOEs were comparable. It was possible to completely and unequivocally assign all of the deoxyribose H2′ H2″, H3′, and H4′ protons from the NOESY data. A partial set of assignments was achieved for the deoxyribose H5′ and H5″ protons. The assignments are tabulated in Table S1 in Supporting Information.

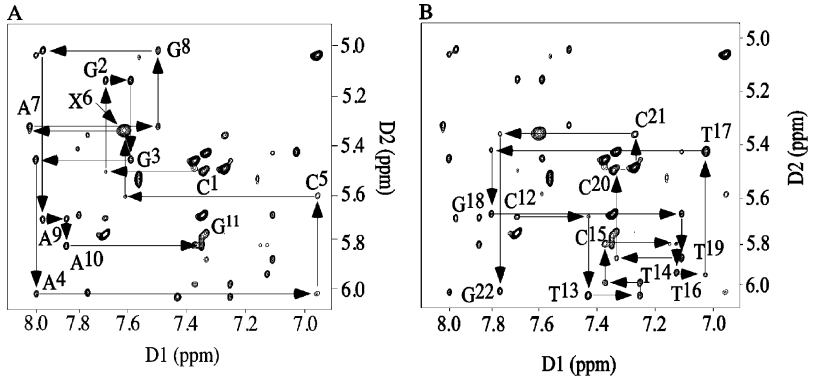

FIGURE 1: Expanded plot of a NOESY spectrum in D_2O buffer (pH 7.0) at a mixing time of 250 ms showing the sequential NOE connectivities between the aromatic and anomeric protons for the *S*-N1−BDO-(61,2) adduct. The base positions are indicated at the intranucleotide cross-peak of the aromatic proton to its own anomeric proton. (A) Sequential NOE connectivities for nucleotides C^1 to G^{11}. (B) Sequential NOE connectivities for nucleotides C^{12} to G^{22}.

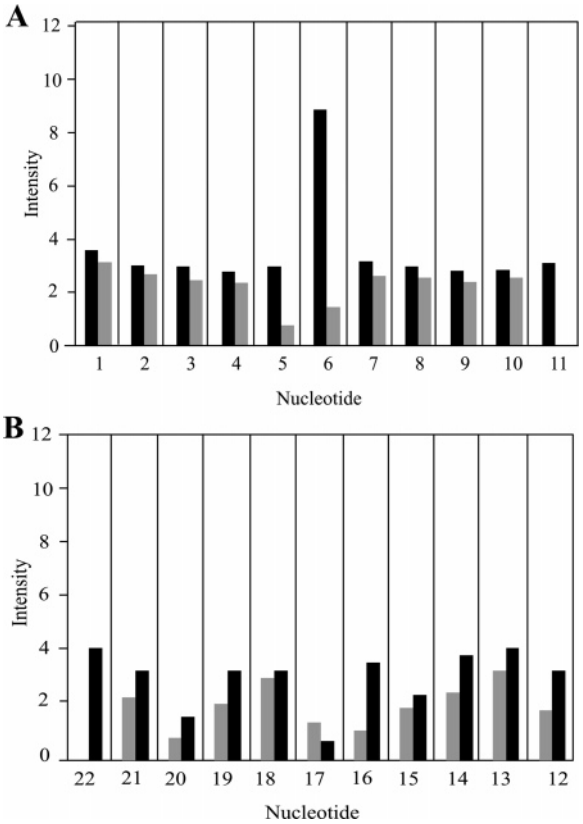

FIGURE 2: Comparison of intensities for the H6/H8 to H1′ interactions of the aromatic and anomeric protons of the (A) modified strand and (B) complementary strand for the *S*-N1−BDO-(61,2) adduct. Black bars represent intraresidue cross-peaks. Gray bars represent interresidue cross-peaks.

Exchangeable Protons. A contour plot of the imino proton region of the NOESY spectrum, ranging from ∼12−15 ppm, is shown in Figure 3. The cross-peaks located in the imino region were well-resolved, with the exception of T^{14} and T^{16}, which overlapped. Cross-peaks arising from the A^7 H2 to T^{16} N3H and A^9 H2 to T^{14} N3H NOEs confirmed that both T^{14} N3H and T^{16} N3H resonated at 13.6 ppm. The resonance arising from T^{17} N3H was not observed, and there was a subsequent break in sequential connectivity between T^{16} N3H and G^{18} N1H. The imino protons of the terminal C^1·G^{22} pair and G^{11}·C^{12} pairs were not detected, presumably due to fraying at the ends of the helices. Otherwise, a complete set of sequential connectivities was observed.

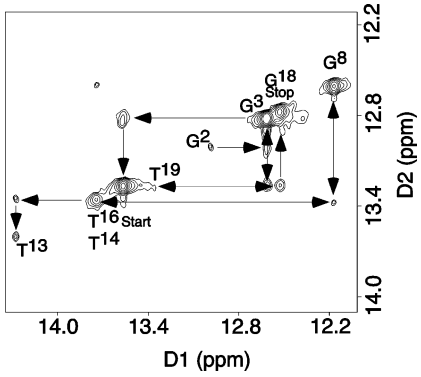

FIGURE 3: Expanded plot of an H_2O NOESY spectrum showing the sequential NOE connectivites for the Watson−Crick base-paired imino protons of the *S*-N1−BDO-(61,2) adduct.

Butadiene Protons. Figure 4 shows the assignment of the butadiene protons from ^{1}H NOESY data. The three butenyl protons,[2] designated H_γ, H_δ, and $H_{\delta'}$ (Scheme 2), were observed between 5 and 6 ppm in the ^{1}H spectrum. The resonance arising from H_γ was observed at 5.79 ppm. The resonance at 5.25 ppm was assigned as arising from $H_{\delta'}$ because it exhibited a stronger NOE with H_γ and with X^6 H2 than did the resonance at 5.12 ppm, which was assigned as H_δ. The H_β proton was assigned at 4.80 ppm. H_β also exhibited an NOE to X^6 H2. It exhibited NOEs to two protons that resonated at 3.22 and 3.40 ppm, which were assigned as the enantiotopic hydroxymethyl $H_{\alpha,\alpha'}$ protons. Their spectral assignments were based upon the predictions of potential energy minimization calculations that predicted that the lowest energy conformation of the *S*-N1−BD moiety placed the C_α hydroxy group such that the hydroxyl proton was within hydrogen bonding distance of the inosine keto oxygen, X^6 O^6. In this conformation H_α was expected to exhibit a stronger NOE to H_δ and a weaker NOE to $H_{\delta'}$, whereas $H_{\alpha'}$ was expected to exhibit only weak NOEs to H_δ and $H_{\delta'}$. Accordingly, the resonance at 3.40 ppm was assigned as H_α and the resonance at 3.22 ppm was assigned as $H_{\alpha'}$.

NOE Connectivities between Butadiene and DNA. Figure 4 also summarizes the NOEs that were observed between the *S*-N1−BDO-(61,2) adduct and the oligodeoxynucleotide. NOEs were observed between the BD $H_{\alpha,\alpha'}$ protons and C^5 H5; the stronger NOE was BD $H_{\alpha'} \rightarrow C^5$ H5. These NOEs established that the hydroxymethyl group of the *S*-N1−BDO-(61,2) adduct was oriented in the 5′ direction in the major

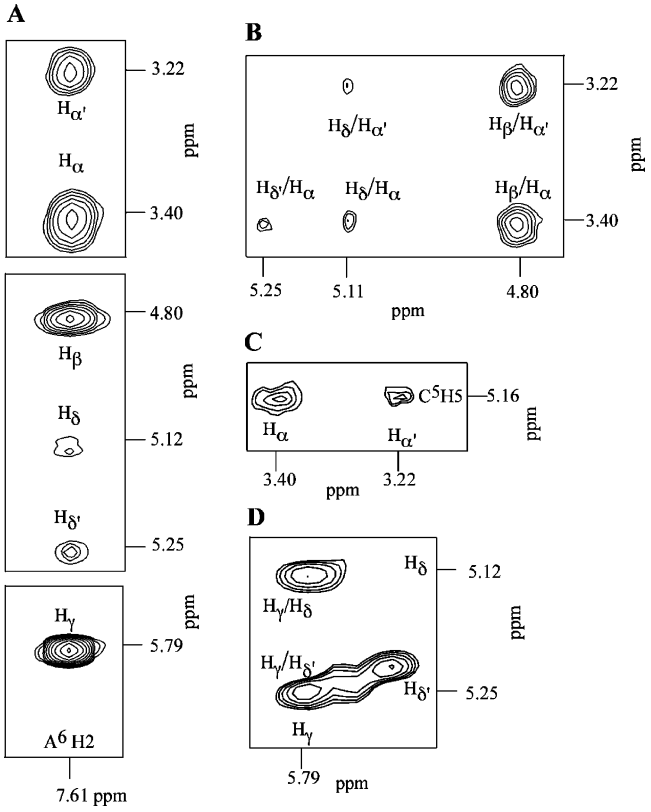

FIGURE 4: Expanded tile plots showing ^{1}H NOEs between the DNA and the butadiene protons for the *S*-N1−BDO-(61,2) adduct. (A) NOEs between the X^6 H2 proton and all the butadiene moiety protons. (B) NOEs between various butadiene protons. (C) NOEs between C^5 H5 and H_s and $H_{s'}$ butadiene protons. (D) NOEs between H_β and H_α and $H_{\alpha'}$.

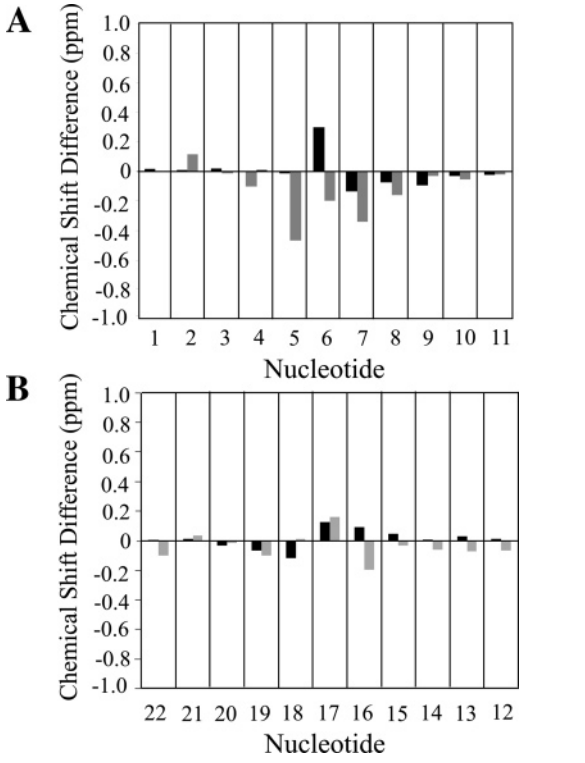

FIGURE 5: Chemical shift differences of aromatic H6 or H8 protons (black bars) and anomeric H1′ protons (gray bars) of the *S*-N1−BDO-(61,2) adduct relative to the unmodified *ras61* oligodeoxynucleotide.

groove. A series of NOEs were observed between X^6 H2 and all of the BD protons. The strongest NOE was observed between X^6 H2 and BD H_γ, with weaker NOEs to H_β, and $H_{\delta,\delta'}$. The latter two NOEs were undoubtedly a result of spin diffusion effects occurring at longer NOE mixing times. The NOEs between X^6 H2 and the enantiotopic $H_{\alpha,\alpha'}$ protons were weak, consistent with the predictions of potential energy minimization calculations that placed $H_{\alpha,\alpha'}$ facing away from X^6 H2. No NOEs were observed between *S*-N1−BDO-(61,2) adduct protons and protons in the complementary strand of the duplex.

Chemical Shift Effects. As shown in Figure 5, only nucleotides C^5, X^6, and A^7 in the modified strand showed significant chemical shift perturbations as compared to the unmodified *ras61* oligodeoxynucleotide (*28*). These perturbations involved the deoxyribose H1′ protons at all three nucleotides, and the imidazole proton X^6 H8 at the adduct site, which shifted upfield 0.2 ppm. The largest chemical shift perturbation was a downfield shift on the order of 0.4 ppm, at C^5 H1′. The complementary strand showed only minor chemical shift perturbations.

Restrained Molecular Dynamics Calculations. NOE-derived distance restraints and empirical data were used to restrain a series of molecular dynamics calculations (Table 1). These rMD calculations employed a simulated annealing protocol. They incorporated 364 NOE-based distance restraints and an additional 90 pseudorotation and 62 empirical phosphodiester backbone angle measurements were also included. Two sets of calculations were completed. In the first, no hydrogen bonding restraints were included at the modified X^6•T^{17} base pair. In the second, an empirical hydrogen bonding restraint between X^6 N7 and T^{17} N3H and was included. Both sets of calculations were initiated using both B-form DNA and A-form DNA starting structures, to ensure that the emergent structures were determined by the experimental restraints and were independent of the respective starting structures. In all instances, the calculations converged successfully to ensembles of similar structures, as indicated by pairwise rmsd comparisons, which were <1 Å, irrespective of A-form or B-form starting structure, or the presence or absence of an empirical hydrogen bonding interaction between X^6 N7 and T^{17} N3H. Figure 6 shows a stereoview of an ensemble of structures that emerged from randomly seeded rMD calculations, which did not include a hydrogen bonding restraint between X^6 N7 and T^{17} N3H. With the exception of the modified base pair X^6•T^{17}, the overall conformation of the oligodeoxynucleotide was more similar to B-form than A-form DNA. This was evidenced by a rmsd of 1.2 Å between the B-form starting structure and the average structure emergent from the rMD calculations, whereas the rmsd between the A-form starting structure and the average structure emergent from the rMD calculations was 6.9 Å.

The accuracies of the structures emergent from both sets of rMD calculations were assessed by complete relaxation matrix calculations using the program CORMA (*36*). These calculations yielded a sixth root residual (R_1^x value) between the NOE intensities predicted by the refined structures and the experimentally measured NOE intensities. The complete relaxation calculations revealed good agreement with experimental NOE data only in the absence of a hydrogen bonding restraint between X^6 N7 and T^{17} N3H. For the rMD

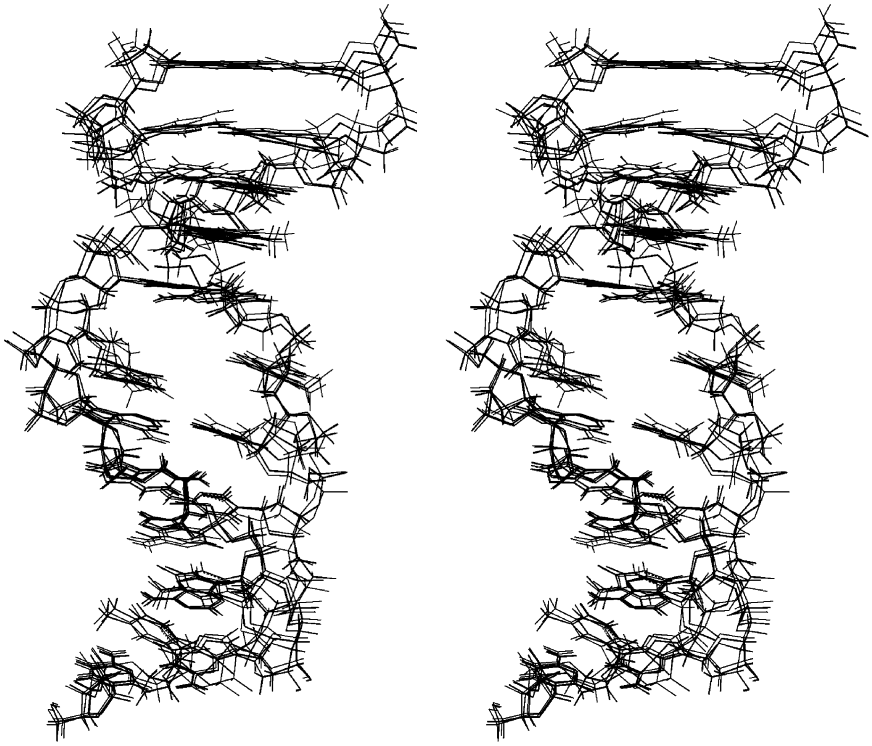

FIGURE 6: A stereoview of six superimposed structures of the *S*-N1−BDO-(61,2) oligodeoxynucleotide emergent from the simulated annealing rMD protocol; the structures resulted from randomly seeded calculations.

Table 1: Root Mean Square (rms) Deviations, Excluding the End Base Pairs, between Various Initial Structures and Intermediate Structures of the *S*-N1−BD Adduct in the Modified Oligodeoxynucleotide

	atomic rms difference (Å)
NMR restraints	
total no. of distance restraints	364
interresidue distance restraints	70
intraresidue distance restraints	294
BD distance restraints	15
deoxyribose pseudorotation restraints	90
backbone torsion angle restraints	62
hydrogen-bonding restraints	6
initial structures	
IniA vs IniB	6.07
rms shifts	
IniA vs <rMDA>[a]	6.89 ± 0.13
IniB vs <rMDB>[b]	1.19 ± 0.10
<rMDB> vs <rMDB>	0.65 ± 0.12
<rMDA> vs <rMDA>	0.78 ± 0.10
RMS pairwise difference (rMDB)	1.02
standard deviation (rMDB)	0.26
RMS difference from mean structure(rMDB)	0.65
standard deviation (rMDB)	0.15

[a] <rMDA> represents the set of six structures that emerged from rMD calculations starting with IniA. [b] <rMDB> represents the set of six structures that emerged from rMD calculations starting from IniB.

calculations that included this hydrogen bonding restraint, the agreement of the emergent structures with NOE data obtained at base pair X^6•T^{17} was poor. Figure 7 shows R_1^x values as a function of position in the *S*-N1−BD oligodeoxynucleotide in the absence of a hydrogen bonding interaction between X^6 N7 and T^{17} N3H. The sixth root residuals were consistently <0.10 at each nucleotide, indicating respectable agreement between the calculated NOE intensities and the experimental NOE intensities.

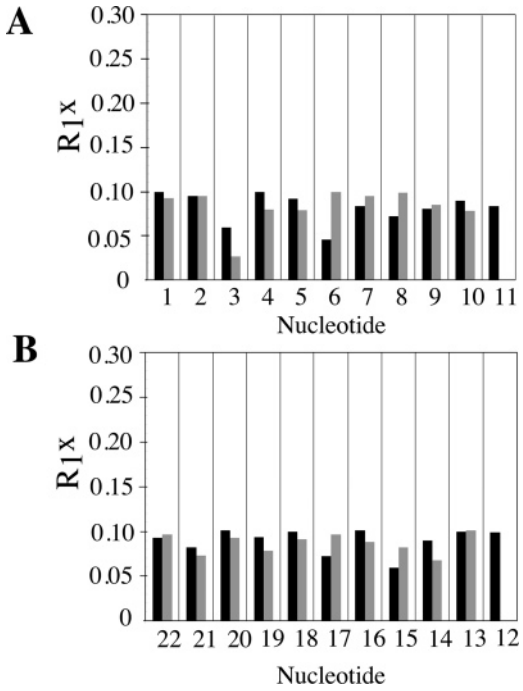

FIGURE 7: Complete relaxation matrix calculations (*36*) on the average structure of the *S*-N1−BDO-(61,2) oligodeoxynucleotide emergent from the simulated annealing rMD protocol showing sixth root residuals (R_1^x) for each nucleotide. (A) The adducted strand. (B) The complementary strand.

Refined Structure. Figure 8 shows a CPK model of the average structure emergent from the structural refinement protocol. The refined structure revealed that the *S*-N1−BDO-(61,2) adduct existed in the high syn conformation about the glycosyl bond, with $\chi = 106°$. In this orientation, X^6 and the BD moiety extended into the major groove of the DNA. The complementary nucleotide T^{17} remained stacked

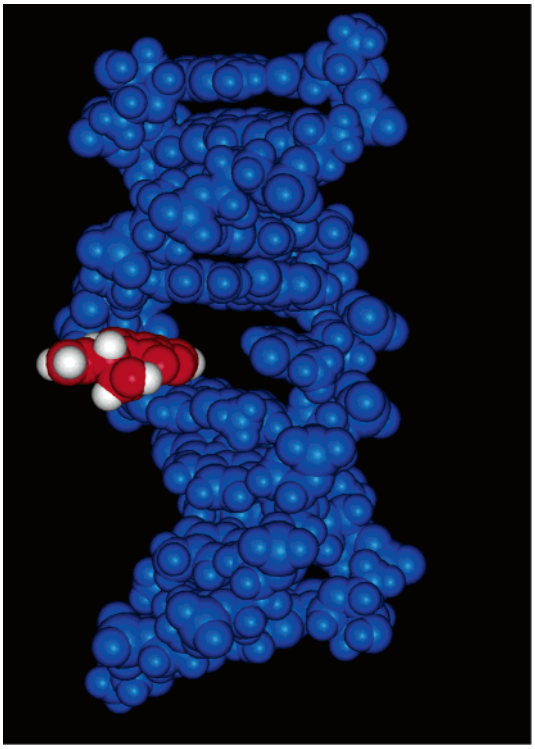

FIGURE 8: A CPK representation of the *S*-N1−BDO-(61,2) oligodeoxynucleotide showing the modified nucleotide X^6 in red, and the BD protons in white; this structure was energy-minimized using the conjugate gradients algorithm.

into the helix despite the fact that the rMD calculations suggested no hydrogen bond was formed between X^6 N7 and T^{17} N3H. In fact, the complementary strand showed little distortion. As shown in Figure 9, the refined structure suggested reduced purine−purine stacking between X^6 and A^7 in the modified strand, as compared to the corresponding stacking interaction between A^6 and A^7 in the unmodified *ras61* oligodeoxynucleotide (*28*). The calculations predicted that rotation of X^6 about the glycosyl bond placed the X^6 H8 proton above the purine ring of A^7, whereas X^6 H2 now faced into the major groove.

DISCUSSION

Epidemiological studies have suggested that chronic human exposure to BD may induce genotoxic effects (*11*−*13*) and is correlated with increased risk for leukemia (*1*, *14*−*22*). This led to the classification of butadiene as "carcinogenic to humans by inhalation" (*9*), and as a "probable human carcinogen" (Group 2A) (*10*). Consequently, the elucidation of structure−activity relationships for adducts arising from the alkylation of DNA by butadiene mono- and diepoxides are of considerable interest. When B6C3F1 *lacI* transgenic mice were exposed to butadiene, it was observed that the adenine-specific point mutations were primarily A to T transversions (*45*−*49*). Significantly, however, A-to-G transitions were reported in *H-ras* codon 61 (*50*).

The identification of the specific adenine adducts that may be responsible for these mutations represents a challenging problem. The oxidative metabolism of butadiene is complex and leads to several different electrophiles, each of which can alkylate multiple sites in DNA. Moreover, there exist multiple stereoisomers of each potential alkylation product. Here we focus on the initially formed product of cytochrome P450 oxidation, butadiene mono epoxide, BDO.

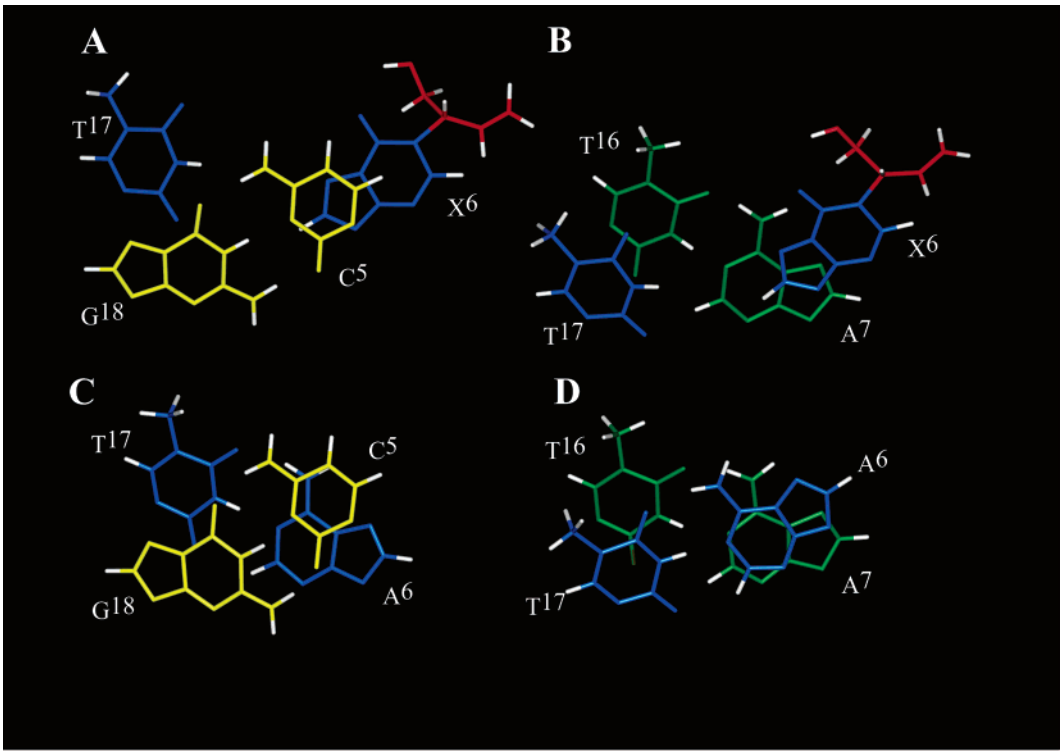

FIGURE 9: A comparison of stacking interactions between the *S*-N1−BDO-(61,2) oligodeoxynucleotide and the corresponding unmodified *ras61* oligodeoxynucleotide. (A) Stacking of base pair C^5•G^{18} (yellow; protons white) above base pair X^6•T^{17} (blue; BD moiety in red; protons white) in the modified oligodeoxynucleotide. (B) Stacking of base pair X^6•T^{17} (blue; BD moiety in red; protons white) above base pair A^7•T^{16} (green; protons white) in the modified oligodeoxynucleotide. (C) Stacking of base pair C^5•G^{18} (yellow; protons white) above base pair A^6•T^{17} (blue; protons white) in the unmodified oligodeoxynucleotide. (D) Stacking of base pair A^6•T^{17} (blue; protons white) above base pair A^7•T^{16} (green; protons white) in the unmodified oligodeoxynucleotide.

Genotoxic Significance of N1-dA Adducts. Alkylation of the adenine N1 imine by BDO can occur at either carbon atom anchoring the oxirane; reaction at the internal carbon, C_β, results in the formation of stereoisomeric N1-(1-hydroxy-3-buten-2-yl)-2′-deoxyadenosine adducts (Scheme 1). These initially formed N1-dA adducts can subsequently undergo rearrangement to the corresponding N1 deoxyinosine adduct, or alternatively, Dimroth rearrangement to the corresponding N^6-dA adducts (*25*, *51*, *52*). Consequently, it has not been possible to examine the initially formed *S*-N1−BDO-(61,2)-dA adduct, either in terms of site-specific mutagenesis or structure. However, two Dimroth rearrangment products arising from alkylation of N1-dA by butadiene diol epoxide (BDE), the N^6-dA butadiene triol (BDT) adducts, were examined, in the *ras61* sequence. They were readily bypassed in *Escherichia coli* and were weakly mutagenic (*53*). Structural studies revealed that they oriented into the major groove, accompanied by modest structural perturbation, although interestingly, the observed structural perturbations were stereospecific (*54*, *55*). The parallel mutagenesis and structural studies on the N^6-dA BDT adducts suggested that to the extent that N1-dA alkylation products represent the source of dA-specific mutations in mice (*45*−*49*), either the N1-dA alkylation products themselves, or their inosine deamination products were likely to represent the more genotoxic species.

Site-specific mutagenesis studies of this N1-(1-hydroxy-3-buten-2-yl)-2′-deoxyinosine adduct in the COS-7 system revealed that it was indeed highly mutagenic, and it yielded A-to-G mutations (*26*, *27*). This led to the proposal (*27*) that deamination of initially formed N1 adducts of BD may represent the source of the *H-ras* specific A-to-G mutations observed in vivo (*50*). Indeed, deamination of dA yields dI and the latter would be expected to code for dCTP insertion during translesion replication. Nevertheless, the observation that the *S*-N1−BDO-(61,2) adduct coded for dCTP (*26*, *27*) was somewhat unexpected, because the presence of the N1 adduct would preclude Watson−Crick type pairing between dCTP and dI in the template strand. It was proposed that perhaps instead the S−N1−BD inosine adduct promotes formation of a Hoogsteen-type pairing interaction with dCTP during trans lesion synthesis (*27*), thus resulting in the observed A-to-G transitions (*50*).

Structural Analysis. The key feature of the *S*-N1−BDO-(61,2) adduct structure was the rotation of the adducted deoxyinosine at X^6 into the high syn conformation about the glycosyl bond, allowing accommodation of the *S*-N1−BDO-(61,2) adduct within the major groove of the DNA. This conformational rearrangement placed X^6 H8 toward the minor groove as opposed to its normal position in the major groove, the result being that the C^5 H1′ to X^6 H8 NOE was abnormally weak. Simultaneously, the reorientation of X^6 placed X^6 H8 proximate to X^6 H1′, but further from X^6 H3′. This resulted in an exceptionally intense NOE cross-peak between X^6 H8 and X^6 H1′ but a weaker than normal cross-peak between X^6 H8 and X^6 H3′ (Figure 2). Subsequent rMD calculations revealed a distance between X^6 H8 and X^6 H1′ < 3.0 Å. The high syn orientation of X^6 also perturbed base−base stacking interactions between base pairs C^5•G^{18}, X^6•T^{17}, and X^7•T^{16}. The changes in these stacking interactions are qualitatively revealed by chemical shift perturbations at nucleotides C^5, X^6, and A^7. As a consequence of the fact that X^6 was in the high syn conformation, X^6 H8 was stacked above A^7 H8, consistent with the 0.2 ppm upfield shift observed for this proton as compared to the unmodified *ras61* oligodeoxynucleotide (*28*). In the high syn conformation, the inosine base does not stack above X^6 H2′, as might be expected for the normal range of the syn conformation for the glycosyl torsion angle. In contrast to the modified strand, the complementary strand was relatively unperturbed by the presence of the *S*-N1−BDO-(61,2) adduct, as compared to the unmodified *ras61* oligodeoxynucleotide (*28*). Potential energy minimization calculations predicted that the hydroxyl group at C_α of the BD moiety should orient toward the inosine keto oxygen, X^6 O^6. This conclusion was supported by the relative magnitudes of NOEs between X^6 H2 and the BD protons, and as well, between the various protons of the butadiene moiety. Formation of a hydrogen bond between the C_α hydroxyl and X^6 O^6 resulted in a stable orientation for the *S*-N1−BDO-(61,2) adduct, consistent with spectral line shapes of the BD protons, which were similar to those arising from oligodeoxynucleotide protons, indicating the BD protons had relaxation properties similar to the protons of the larger oligodeoxynucleotide. In this orientation BD H_γ was positioned in the same plane as X^6 H2, consistent with the strong NOE observed between these two protons. This orientation also accounted for the distinct chemical shift environments of the enantiotopic $H_{\alpha,\alpha'}$ protons. NOEs observed between $H_{\alpha,\alpha'}$ and C^5 H5 clearly positioned the hydroxymethyl group of the *S*-N1−BD adduct in the 5′ direction with respect to X^6. Watson−Crick base pairing was interrupted at the X^6•T^{17} pair, due to reorientation of X^6 into the high syn conformation about the glycosyl bond. Despite this, its complementary nucleotide T^{17} remained intrahelical. However, in the high syn conformation for the glycosyl bond, X^6 was extruded into the major groove, leaving T^{17} exposed to solvent. Inspection of Figure 8 reveals that this structure results in formation of a solvent accessible "hole" in the duplex at the lesion site. This was consistent with the observation that the resonance arising from T^{17} N3H was not observable (Figure 3) presumably due to rapid exchange with solvent. The results of rMD calculations suggested that X^6 N7 was not hydrogen bonded to T^{17} N3H. Thus, the intrahelical orientation of T^{17} appears to be the consequence of favorable free energy arising from its interaction with the more hydrophobic intrahelical environment.

Structure−Activity Relationship. The present results suggest the N1-dI deamination products as a potential source of A → G transitions in *H-ras* codon 61 (*50*). The rotation of the *S*-N1−BDO-(61,2) adduct into the high syn conformation about the glycosyl bond potentially positions it to form a protonated Hoogsteen pairing interaction with incoming dCTP during translesion DNA replication, as had been previously proposed (*26*, *27*) (Scheme 3). The location of the BD moiety in the major groove and distal to the Hoogsteen-binding face of the *S*-N1−BDO-(61,2) adduct suggests that a protonated Hoogsteen pair could form during lesion bypass. Thus, it will now be of interest to examine the *S*-N1−BDO-(61,2) adduct opposite dC in the complementary strand, to examine whether it does stabilize formation of a protonated Hoogsteen pairing interaction.

Comparison with 1,N^6-Ethenodeoxyadenosine Adducts. The exocyclic 1,N^6-ethenodeoxyadenosine adduct, 1,N^6-ϵdA, provides an interesting comparison with the *S*-N1−BDO-

Scheme 3: (A) Formation of a Protonated Hoogsteen Pair between the N1-(1-Hydroxy-3-buten-2(*S*)-yl)-2′-Deoxyinosine Adduct and Cytosine. (B) Formation of a Protonated Hoogsteen Pair between the 1,N^6-ϵdA Adduct and Cytosine. (C) Formation of a dG(anti)·1,N^6-ϵdA(syn) Base Pair (*60*)

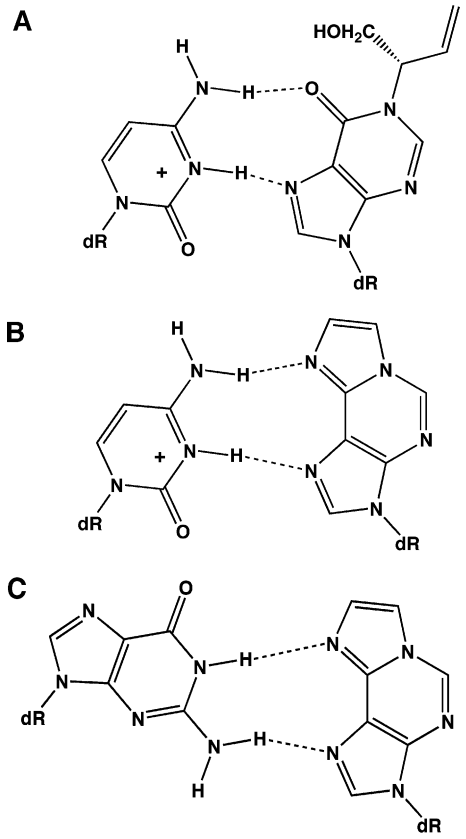

(61,2) adduct studied in this work. In this exocyclic adduct N^6 becomes a hydrogen bond acceptor rather than a hydrogen bond donor, similar to O^6 in the *S*-N1−BDO-(61,2) deoxyinosine adduct. Site-specific mutagenesis studies using 1,N^6-ϵdA were conducted in *Escherichia coli* (*56*), in COS-7 (*57*), and in human cells (*56*, *58*). The mutagenic response differed somewhat in these systems. However, similar to the *S*-N1−BDO-(61,2) dI adduct, in the COS-7 system, 1,N^6-ϵdA induced primarily A-to-G transitions (*57*), and the mutations observed in human cells also included A-to-G transitions (*56*, *58*), suggesting a propensity for misincorporation of dCTP opposite the adduct. Rotation of 1,N^6-ϵdA into the syn conformation during trans-lesion replication would potentially allow it to pair with incoming protonated dCTP as we propose for the *S*-N1−BDO-(61,2) adduct or alternatively, with incoming dGTP (Scheme 3).

The available structural data for the 1,N^6-ϵdA adduct suggest a complex interplay of factors controlling the interconversion of the exocyclic adduct between the syn and anti conformations about the glycosyl bond. When placed opposite thymidine in duplex DNA, the 1,N^6-ϵdA adduct differed from the *S*-N1−BDO-(61,2) deoxyinosine adduct—it remained in the anti conformation about the glycosyl bond (*59*). However, in solution, an 1,N^6-ϵdA·dG mismatch was observed with 1,N^6-ϵdA in the syn conformation about the glycosyl bond (*60*), although this was not corroborated by crystallographic analysis (*61*). The 1,N^6-ϵdA·C mismatch has not been examined.

SUMMARY

When placed opposite T in duplex DNA, the deamination product of the N1-(1-hydroxy-3-buten-2(*S*)-yl)-2′-deoxyadenosine adduct, N1-(1-hydroxy-3-buten-2(*S*)-yl)-2′-deoxyinosine, exists in the high syn conformation about the glycosyl bond, with the glycosyl torsion angle χ in the range of 106°. The thymine complementary to the N1-modified deoxyinosine remains intrahelical. We propose that rotation of this adduct into the high syn conformation facilitates incorporation of dCTP during trans-lesion replication, thus generating A-to-G mutations, which have been observed site-specific mutagenesis studies (*26*, *27*).

ACKNOWLEDGMENT

Mr. Markus Voehler and Dr. Jaison Jacob assisted with NMR spectroscopy. Dr. Jarrod Smith assisted with structural refinement.

SUPPORTING INFORMATION AVAILABLE

^{1}H chemical shift assignments for the *S*-N1−BDO-(61,2) adduct (Table S1), the NOE restraints utilized in the rMD calculations for the *S*-N1−BDO-(61,2) adduct (Table S2), and force field parametrization and partial charges for the *S*-N1−BDO-(61,2) adduct (Table S3). This material is available free of charge via the Internet at http://pubs.acs.org.

REFERENCES

1. Himmelstein, M. W., Acquavella, J. F., Recio, L., Medinsky, M. A., and Bond, J. A. (1997) Toxicology and epidemiology of 1,3-butadiene. *Crit. Rev. Toxicol. 27*, 1−108.
2. Jackson, M. A., Stack, H. F., Rice, J. M., and Waters, M. D. (2000) A review of the genetic and related effects of 1,3-butadiene in rodents and humans. *Mutat. Res. 463*, 181−213.
3. Pelz, N., Dempster, N. M., and Shore, P. R. (1990) Analysis of low molecular weight hydrocarbons including 1,3-butadiene in engine exhaust gases using an aluminum oxide porous-layer open-tubular fused-silica column. *J. Chromatogr. Sci. 28*, 230−235.
4. Brunnemann, K. D., Kagan, M. R., Cox, J. E., and Hoffmann, D. (1990) Analysis of 1,3-butadiene and other selected gas-phase components in cigarette mainstream and sidestream smoke by gas chromatography−mass selective detection. *Carcinogenesis 11*, 1863−1868.
5. Huff, J. E., Melnick, R. L., Solleveld, H. A., Haseman, J. K., Powers, M., and Miller, R. A. (1985) Multiple organ carcinogenicity of 1,3-butadiene in B6C3F1 mice after 60 weeks of inhalation exposure. *Science 227*, 548−549.
6. Melnick, R. L., Huff, J., Chou, B. J., and Miller, R. A. (1990) Carcinogenicity of 1,3-butadiene in C57BL/6 x C3H F1 mice at low exposure concentrations. *Cancer Res. 50*, 6592−6599.
7. Melnick, R. L., Huff, J. E., Roycroft, J. H., Chou, B. J., and Miller, R. A. (1990) Inhalation toxicology and carcinogenicity of 1,3-butadiene in B6C3F1 mice following 65 weeks of exposure. *Environ. Health Perspect. 86*, 27−36.
8. Owen, P. E., and Glaister, J. R. (1990) Inhalation toxicity and carcinogenicity of 1,3-butadiene in Sprague−Dawley rats. *Environ. Health Perspect. 86*, 19−25.
9. United States Environmental Protection Agency (2002) 1,3-Butadiene. Carcinogenicity assessment for lifetime exposure: Weight-of-evidence characterization, available at http://www.epa.gov/iris/subst/0139.htm.
10. International Agency for Research on Cancer (1999) Re-evaluation of some organic chemicals, hydrazine and hydrogen peroxide, IRC Monographs on the Evaluation of Carcinogenic Risks to Humans. *IARC Sci. Publ. 71*, 109−125.
11. Ward, J. B., Jr., Ammenheuser, M. M., Bechtold, W. E., Whorton, E. B., Jr., and Legator, M. S. (1994) hprt mutant lymphocyte frequencies in workers at a 1,3-butadiene production plant. *Environ. Health Perspect. 102 Suppl. 9*, 79−85.

12. Ward, J. B., Jr., Ammenheuser, M. M., Whorton, E. B., Jr., Bechtold, W. E., Kelsey, K. T., and Legator, M. S. (1996) Biological monitoring for mutagenic effects of occupational exposure to butadiene. *Toxicology 113*, 84−90.
13. Sram, R. J., Rossner, P., Peltonen, K., Podrazilova, K., Mrackova, G., Demopoulos, N. A., Stephanou, G., Vlachodimitropoulos, D., Darroudi, F., and Tates, A. D. (1998) Chromosomal aberrations, sister-chromatid exchanges, cells with high frequency of SCE, micronuclei and comet assay parameters in 1,3-butadiene-exposed workers. *Mutat. Res. 419*, 145−154.
14. Delzell, E., Sathiakumar, N., Hovinga, M., Macaluso, M., Julian, J., Larson, R., Cole, P., and Muir, D. C. (1996) A follow-up study of synthetic rubber workers. *Toxicology 113*, 182−189.
15. Meinhardt, T. J., Lemen, R. A., Crandall, M. S., and Young, R. J. (1982) Environmental epidemiologic investigation of the styrene-butadiene rubber industry. Mortality patterns with discussion of the hematopoietic and lymphatic malignancies. *Scand. J. Work. Environ. Health 8*, 250−259.
16. Matanoski, G., Francis, M., Correa-Villasenor, A., Elliott, E., Santos-Burgoa, C., and Schwartz, L. (1993) Cancer epidemiology among styrene-butadiene rubber workers. *IARC Sci. Publ. 127*, 363−374.
17. Santos-Burgoa, C., Matanoski, G. M., Zeger, S., and Schwartz, L. (1992) Lymphohematopoietic cancer in styrene-butadiene polymerization workers. *Am. J. Epidemiol. 136*, 843−854.
18. Macaluso, M., Larson, R., Delzell, E., Sathiakumar, N., Hovinga, M., Julian, J., Muir, D., and Cole, P. (1996) Leukemia and cumulative exposure to butadiene, styrene and benzene among workers in the synthetic rubber industry. *Toxicology 113*, 190−202.
19. Matanoski, G. M., and Schwarts, L. (1987) Mortality of workers in styrene-butadiene polymer production. *J. Occup. Med. 29*, 675−680.
20. Santos-Burgoa, C., Eden-Wynter, R. A., Riojas-Rodriguez, H., and Matanoski, G. M. (1997) Living in a chemical world. Health impact of 1,3-butadiene carcinogenesis. *Ann. N. Y. Acad. Sci. 837*, 176−188.
21. Matanoski, G., Elliott, E., Tao, X., Francis, M., Correa-Villasenor, A., and Santos-Burgoa, C. (1997) Lymphohematopoietic cancers and butadiene and styrene exposure in synthetic rubber manufacture. *Ann. N. Y. Acad. Sci. 837*, 157−169.
22. Albertini, R., Clewell, H., Himmelstein, M. W., Morinello, E., Olin, S., Preston, J., Scarano, L., Smith, M. T., Swenberg, J., Tice, R., and Travis, C. (2003) The use of non-tumor data in cancer risk assessment: Reflections on butadiene, vinyl chloride, and benzene. *Regul. Toxicol. Pharmacol. 37*, 105−132.
23. Csanady, G. A., Guengerich, F. P., and Bond, J. A. (1992) Comparison of the biotransformation of 1,3-butadiene and its metabolite, butadiene monoepoxide, by hepatic and pulmonary tissues from humans, rats and mice [published erratum appears in Carcinogenesis (1993) *14*, 784] *Carcinogenesis 13*, 1143−1153.
24. Duescher, R. J., and Elfarra, A. A. (1994) Human liver microsomes are efficient catalysts of 1,3-butadiene oxidation: Evidence for major roles by cytochromes P450 2A6 and 2E1. *Arch. Biochem. Biophys. 311*, 342−349.
25. Selzer, R. R., and Elfarra, A. A. (1996) Characterization of N1- and N^6-adenosine adducts and N1-inosine adducts formed by the reaction of butadiene monoxide with adenosine: Evidence for the N1-adenosine adducts as major initial products, *Chem. Res. Toxicol. 9*, 875−881.
26. Rodriguez, D. A., Kowalczyk, A., Ward, J. B. J., Harris, C. M., Harris, T. M., and Lloyd, R. S. (2001) Point mutations induced by 1,2-epoxy-3-butene N1 deoxyinosine adducts. *Environ. Mol. Mutagen. 38*, 292−296.
27. Kanuri, M., Nechev, L. V., Tamura, P. J., Harris, C. M., Harris, T. M., and Lloyd, R. S. (2002) Mutagenic spectrum of butadiene-derived N1-deoxyinosine adducts and N^6,N^6-deoxyadenosine intrastrand cross-links in mammalian cells. *Chem. Res. Toxicol. 15*, 1572−1580.
28. Feng, B., and Stone, M. P. (1995) Solution structure of an oligodeoxynucleotide containing the human N-ras codon 61 sequence refined from ^{1}H NMR using molecular dynamics restrained by nuclear Overhauser effects. *Chem. Res. Toxicol. 8*, 821−832.
29. Borer, P. N. (1975) in *Handbook of Biochemistry and Molecular Biology*, CRC Press, Cleveland, OH.
30. Kowalczyk, A., Harris, C. M., and Harris, T. M. (2001) Synthesis and characterization of oligodeoxynucleotides containing an N1 β-hydroxyalkyl adduct of 2′-deoxyinosine. *Chem. Res. Toxicol. 14*, 746−753.
31. Piotto, M., Saudek, V., and Sklenar, V. (1992) Gradient-tailored excitation for single-quantum NMR spectroscopy of aqueous solutions. *J. Biomol. NMR 6*, 661−665.
32. Bax, A., and Davis, D. G. (1985) MLEV-17-based two-dimensional homonuclear magnetization transfer spectroscopy. *J. Magn. Reson. 65*, 355−360.
33. Arnott, S., and Hukins, D. W. L. (1972) Optimised parameters for A-DNA and B-DNA. *Biochem. Biophys. Res. Commun. 47*, 1504−1509.
34. Brunger, A. T. (1992) *X-Plor. Version 3.1. A system for X-ray Crystallography and NMR*, Yale University Press, New Haven, CT.
35. James, T. L. (1991) Relaxation matrix analysis of two-dimensional nuclear Overhauser effect spectra. *Curr. Opin. Struct. Biol. 1*, 1042−1053.
36. Keepers, J. W., and James, T. L. (1984) A theoretical study of distance determination from NMR. Two-dimensional nuclear Overhauser effect spectra. *J. Magn. Reson. 57*, 404−426.
37. Borgias, B. A., and James, T. L. (1989) Two-dimensional nuclear Overhauser effect: Complete relaxation matrix analysis. *Methods Enzymol. 176*, 169−183.
38. Borgias, B. A., and James, T. L. (1990) MARDIGRAS− A procedure for matrix analysis of relaxation for discerning geometry of an aqueous structure. *J. Magn. Reson. 87*, 475−487.
39. Liu, H., Spielmann, H. P., Ulyanov, N. B., Wemmer, D. E., and James, T. L. (1995) Interproton distance bounds from 2D NOE intensities: Effect of experimental noise and peak integration errors. *J. Biomol. NMR 6*, 390−402.
40. Clore, G. M., Brunger, A. T., Karplus, M., and Gronenborn, A. M. (1986) Application of molecular dynamics with interproton distance restraints to three-dimensional protein structure determination. *J. Mol. Biol. 191*, 523−551.
41. Ryckaert, J.-P., Ciccotti, G., and Berendsen, H. J. C. (1977) Numerical integration of the cartesian equations of motion of a system with constraints: Molecular dynamics of n-alkanes. *J. Comput. Phys. 23*, 327−341.
42. Berendsen, H. J. C., Postma, J. P. M., van Gunsteren, W. F., DiNola, A., and Haak, J. R. (1984) Molecular dynamics with coupling to an external bath. *J. Phys. Chem. 81*, 3684−3690.
43. Keepers, J., Kollman, P. A., and James, T. L. (1984) Molecular mechanical studies of base-pair opening in d(CGCGC):d(GCGCG), dG5:dC5, d(TATAT):d(ATATA), and dA5:dT5 in the B and Z forms of DNA. *Biopolymers 23*, 2499−2511.
44. Lu, X. J., and Olson, W. K. (2003) 3DNA: A software package for the analysis, rebuilding and visualization of three-dimensional nucleic acid structures. *Nucleic Acids Res. 31*, 5108−5121.
45. Recio, L., Saranko, C. J., and Steen, A. M. (2000) 1,3-butadiene: Cancer, mutations, and adducts. Part II: Roles of two metabolites of 1,3-butadiene in mediating its in vivo genotoxicity. *Res. Rep. Health Eff. Inst. 92*, 49−87; discussion 141−149.
46. Recio, L., Steen, A. M., Pluta, L. J., Meyer, K. G., and Saranko, C. J. (2001) Mutational spectrum of 1,3-butadiene and metabolites 1,2-epoxybutene and 1,2,3,4-diepoxybutane to assess mutagenic mechanisms. *Chem. Biol. Interact. 135*−*136*, 325−341.
47. Sisk, S. C., Pluta, L. J., Bond, J. A., and Recio, L. (1994) Molecular analysis of lacI mutants from bone marrow of B6C3F1 transgenic mice following inhalation exposure to 1,3-butadiene. *Carcinogenesis 15*, 471−477.
48. Recio, L., and Meyer, K. G. (1995) Increased frequency of mutations at A:T base pairs in the bone marrow of b6c3f1 laci transgenic mice exposed to 1,3-butadiene. *Environ. Mol. Mutagen. 26*, 1−8.
49. Steen, A. M., Meyer, K. G., and Recio, L. (1997) Analysis of hprt mutations occurring in human TK6 lymphoblastoid cells following exposure to 1,2,3,4-diepoxybutane. *Mutagenesis 12*, 61−67.
50. Goodrow, T. L., Nichols, W. W., Storer, R. D., Anderson, M. W., and Maronpot, R. R. (1994) Activation of H-ras is prevalent in 1,3-butadiene-induced and spontaneously occurring murine Harderian gland tumors. *Carcinogenesis 15*, 2665−2667.
51. Barlow, T., Takeshita, J., and Dipple, A. (1998) Deamination and Dimroth rearrangement of deoxyadenosine-styrene oxide adducts in DNA. *Chem. Res. Toxicol. 11*, 838−845.
52. Kim, H. Y., Finneman, J. I., Harris, C. M., and Harris, T. M. (2000) Studies of the mechanisms of adduction of 2′-deoxyadenosine with styrene oxide and polycyclic aromatic hydrocarbon dihydrodiol epoxides. *Chem. Res. Toxicol. 13*, 625−637.

53. Carmical, J. R., Nechev, L. V., Harris, C. M., Harris, T. M., and Lloyd, R. S. (2000) Mutagenic potential of adenine N^6 adducts of monoepoxide and diolepoxide derivatives of butadiene. *Environ. Mol. Mutagen. 35*, 48−56.
54. Scholdberg, T. A., Nechev, L. V., Merritt, W. K., Harris, T. M., Harris, C. M., Lloyd, R. S., and Stone, M. P. (2004) Structure of a site-specific major groove (2*S*,3*S*)-N^6-(2,3,4-Trihydroxybutyl)-2′-deoxyadenosyl DNA adduct of butadiene diol epoxide. *Chem. Res. Toxicol. 17*, 717−730.
55. Merritt, W. K., Scholdberg, T. A., Nechev, L. V., Harris, T. M., Harris, C. M., Lloyd, R. S., and Stone, M. P. (2004) Stereospecific structural perturbations arising from adenine N^6 butadiene triol adducts in duplex DNA. *Chem. Res. Toxicol. 17*, 1007−1019.
56. Levine, R. L., Yang, I. Y., Hossain, M., Pandya, G. A., Grollman, A. P., and Moriya, M. (2000) Mutagenesis induced by a single 1,N^6-ethenodeoxyadenosine adduct in human cells. *Cancer Res. 60*, 4098−4104.
57. Pandya, G. A., and Moriya, M. (1996) 1,N^6-ethenodeoxyadenosine, a DNA adduct highly mutagenic in mammalian cells. *Biochemistry 35*, 11487−11492.
58. Basu, A. K., McNulty, J. M., and McGregor, W. G. (1999) Solution conformation and mutagenic specificity of 1,N^6-ethenoadenine. *IARC Sci. Publ. 150*, 325−333.
59. Kouchakdjian, M., Eisenberg, M., Yarema, K., Basu, A., Essigmann, J., and Patel, D. J. (1991) NMR studies of the exocyclic 1,N^6-ethenodeoxyadenosine adduct (ϵdA) opposite thymidine in a DNA duplex. Nonplanar alignment of ϵdA(anti) and dT(anti) at the lesion site. *Biochemistry 30*, 1820−1828.
60. De Los Santos, C., Kouchakdjian, M., Yarema, K., Basu, A., Essigmann, J., and Patel, D. J. (1991) NMR studies of the exocyclic 1,N^6-ethenodeoxyadenosine adduct (ϵdA) opposite deoxyguanosine in a DNA duplex. ϵdA(syn):dG(anti) pairing at the lesion site. *Biochemistry 30*, 1828−1835.
61. Leonard, G. A., McAuley-Hecht, K. E., Gibson, N. J., Brown, T., Watson, W. P., and Hunter, W. N. (1994) Guanine-1,N^6-ethenoadenine base pairs in the crystal structure of d(CGCGAATT-(ϵdA)GCG). *Biochemistry 33*, 4755−4761.

BI0482452